R-10-64

# Creep testing of nodular iron at ambient and elevated temperatures

Åsa Martinsson, Henrik C.M. Andersson-Östling,
Facredin Seitisleam, Rui Wu, Rolf Sandström
Swerea KIMAB AB

December 2010

**Svensk Kärnbränslehantering AB**
Swedish Nuclear Fuel
and Waste Management Co

Box 250, SE-101 24 Stockholm
Phone +46 8 459 84 00

ISSN 1402-3091
SKB R-10-64

# Creep testing of nodular iron at ambient and elevated temperatures

Åsa Martinsson, Henrik C.M. Andersson-Östling,
Facredin Seitisleam, Rui Wu, Rolf Sandström
Swerea KIMAB AB

December 2010

This report concerns a study which was conducted for SKB. The conclusions and viewpoints presented in the report are those of the authors. SKB may draw modified conclusions, based on additional literature sources and/or expert opinions.

A pdf version of this document can be downloaded from www.skb.se.

# Abstract

The creep strain at room temperature, 100 and 125°C has been investigated for the ferritic nodular cast iron insert intended for use as the load-bearing part of canisters for long term disposal of spent nuclear fuel. The microstructure consisted of ferrite, graphite nodules of different sizes, compacted graphite and pearlite. Creep tests have been performed for up to 41,000 h. The specimens were cut out from material taken from two genuine inserts, I30 and I55. After creep testing, the specimens from the 100°C tests were hardness tested and a metallographic examination was performed. Creep strains at all temperatures appear to be logarithmic, and accumulation of creep strain diminishes with time. The time dependence of the creep strain is consistent to the W-model for primary creep. During the loading plastic strains up to 1% appeared. The maximum recorded creep strain after the loading phase was 0.025%. This makes the creep strains technically insignificant. Acoustic emission recordings during the loading of the room temperature tests showed no sounds or other evidence of microcracking during the loading phase. There is no evidence that the hardness or the graphite microstructure changed during the creep tests.

# Contents

# 1 Background

In Sweden, spent nuclear fuel will be stored in basins during the first 30 years. During this time the radioactivity decreases to approximately 1% of the original value, making final disposal possible. The plan for the subsequent and final part of the long term disposal is to encapsulate the spent fuel in canisters designed to sustain at least 100,000 years deep in the bedrock /1/.

The canister consists of an inner, load-bearing part of nodular cast iron and an outer shell made of oxygen-free copper that will act as corrosion barrier, Figure 1-1. The canisters will be placed 500 m down in the bedrock. The space around the canister in the deposition hole will be filled with bentonite clay. /2/ The canister has to withstand stresses during e.g. an earthquake or glaciations. The maximum external pressure is estimated not to exceed 45 MPa /3/ during the long term disposal. Another condition that has to be taken into consideration is the temperature. The decay power of the nuclear waste will imply an enhanced temperature in the nodular iron of up to 125°C /2/. Combined with the external, static stress, this condition will induce creep in the material.

Limited research has so far been performed on creep in nodular cast iron. In /4/ and /5/ creep data in the temperature range 370 to 650°C for a 0.8% Mo iron have been generated. Angus attempts to extrapolate his high temperature data to lower temperatures using a non-conventional and nowadays unacceptable procedure /6/. Röhrig presents creep tests at 705 and 815°C for 4% Si iron with 0 to 2% Mo /7/. He demonstrates that the creep rupture strength increases with increasing Mo content.

Usami et al. /8/ have studied creep in austenitic and low-alloyed steels between –270 and +300°C. They concluded that logarithmic creep occurred in all tested steels in that temperature range. Their study shows that all tested steels have produced a noticeable creep strain at both –196°C and room temperature.

Since no creep results from experiments below 300°C have been found for nodular cast iron, Swedish Nuclear Fuel and Waste Management Co (SKB) decided to initiate a study on the nodular iron used in the insert. The aim of this work is to document the creep resistance at room temperature, 100°C and 125°C and how the microstructure is affected by these conditions.


***Figure 1-1.*** *Canister for final disposal of spent nuclear fuel.*

# 2 Material

## 2.1 Chemical composition

The investigated material is a ferritic nodular cast iron, EN-GJS-400-15U in SS-EN 1563 /9/. Specimens have been taken from two inserts designated I30 and I55. The microstructure is illustrated in Figure 2-1. The chemical composition for the ductile iron used in this investigation is given in Table 2-1. It is a standard material commonly used in both smaller and larger components than the canister inserts.

**Table 2-1. The chemical composition of the nodular iron, wt%.**

| Insert | C | Si | Mn | P | S | Cr | Ni | Mg |
|---|---|---|---|---|---|---|---|---|
| I30 | 3.71 | 2.33 | 0.22 | < 0.003 | 0.005 | 0.03 | 0.65 | – |
| I55 | 3.64 | 2.28 | 0.14 | 0.027 | 0.006 | 0.03 | 0.039 | 0.044 |
| **Insert** | **Mo** | **Cu** | **Sn** | **Ti** | **V** | **$C_{ekv}$*** | **Fe** | |
| I30 | < 0.01 | 0.03 | 0.005 | 0.006 | 0.011 | 4.29 | bal | |
| I55 | 0.00 | 0.035 | – | – | – | 4.22 | bal | |

*$C_{ekv}$=%C+(%Si/4)+(%P/2).

## 2.2 Mechanical properties

According to EN-GJS-400-15U (cast-on samples) the minimum values of the yield and tensile strength are 240 and 370 MPa, respectively. These values are valid for samples taken from the insert. The min elongation for the insert is specified to 7% /SKBdoc 1175208/. The measured tensile properties and the Brinell hardness /10/ are given in Table 2-2.

**Table 2-2. Mechanical properties of the nodular iron in the inserts.**

| Insert | Yield strength, MPa | Tensile strength, MPa | Elongation, % | Brinell hardness |
|---|---|---|---|---|
| EN-GJS-400-15U | ≥ 240 | ≥ 370 | ≥ 11 | – |
| I30 | 283[a] | 390[a] | 11[a] | 148[c] |
| I55 | 276[b] | 398[b] | 16[b] | 146[c] |

a) Average of 7 values; b) Average of 6 values; c) Average of 2 values.

## 2.3 Microstructure

The shape and distribution of the graphite is important for the mechanical properties. The typical form of the graphite is illustrated in Figure 2-1. Nodular graphite dominates the structure. Graphite characterisation according to SS-EN ISO 945-1:2008 /11/ is presented in Table 2-3.

**Table 2-3. Graphite characterisation according to SS-EN ISO 945-1:2008 /11/.**

| Inserts | Nodularity[a] | Nodule density, 1/mm² | Graphite size | Pearlite content, % |
|---|---|---|---|---|
| SS-EN ISO 945-1:2008 | ≥ 80 | | | |
| I30 (two sections) | 90, 95 | 65, 100 | 5/6, 6 | < 1 |
| I55 (two sections) | 90 | 58, 61 | 5/6 | < 5 |

a) Nodularity is the fraction of nodules of type V and VI in percent.

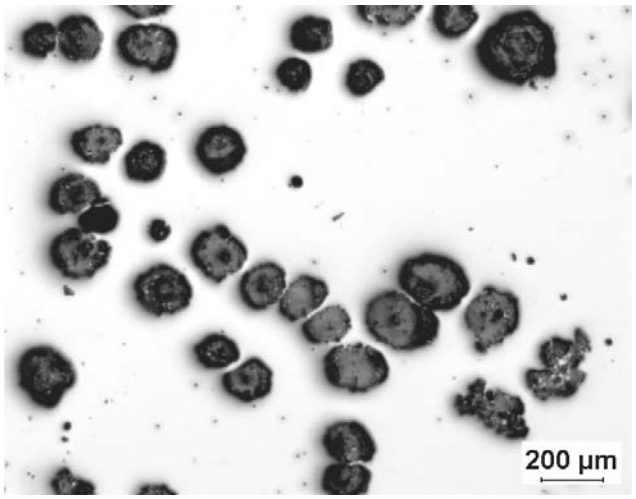


***Figure 2-1.*** *Typical form of graphite in insert No I30. Unetched sample.*

A high fraction of the graphite should have nodular shape, i.e. form V or VI defined in 945-1: 2008 /11/. The inspected micrographs fulfil the requirement that there should be minimum 80% of graphite form V and VI /11/. The nodular density is in the interval 58 to 100 nodules per $mm^2$. The pearlite content is a little bit higher in I55 than in I30, but in both cases less than 5%.

# 3 Experimental

## 3.1 Creep tests

Creep tests were performed at room temperature, 100 and 125°C. All tests were carried out using cylindrical creep specimens with 10 mm diameter and 75 mm gauge length. The test matrix is shown in Table 3-1. Test samples were taken from insert No I30 and I55.

The test machines were of the standard lever arm type with temperature controlled to within ± 1°C both axially and over time. The applied load was controlled to within ± 10 N and strain to within ± 0.1 µm.

The material for the room temperature and 125°C tests was taken from the insert I55, Figure 3-1. A 200 mm thick disc was taken from the middle of the insert, 1,825 mm above the bottom. The triangular shaped blocks shown in Figure 3-1a were used to cut blanks for the specimens. The specimens for the room temperature and 125°C tests were taken in the axial and tangential direction, respectively. In an X-ray examination before testing, these blanks were found to be almost defect free.

The 100°C specimens were taken from an insert cast from Guldsmedshytte Bruks AB identified with the marking I30. The blanks were cut from the bottom part of the insert in the radial direction, Figure 3-1b. X-ray examination of the blanks before testing was made to ensure that the material was free from defects. After testing, the specimens were prepared for metallographic examination, see below.

**Table 3-1. Test matrix for nodular iron creep tests.**

| Test ID | Insert ID | Test type | Temp. °C | Stress, MPa | Load. Time, min | Load. strain, % | Testing time, h | Status | k, eq. 2 $\times 10^{-5}$ |
|---|---|---|---|---|---|---|---|---|---|
| GAE1 | I55 | Creep and acoustic emission measurement | RT | 280 | 10 | 0.54 | 2,302 | Interrupted | |
| GAE2 | | | RT | 260 | 10 | 0.27 | 2,276 | Interrupted | 0.2 |
| GAE3 | | | RT | 240 | 10 | 0.18 | 2,276 | Interrupted | |
| GAE4 | | | RT | 220 | 10 | 0.15 | 2,275 | Interrupted | 0.4 |
| GAE5 | | | RT | 200 | 10 | 0.11 | 2,275 | Interrupted | |
| GAE6 | | | 100 | 200 | 10 | – | 0 | Loading test | |
| G1 | I30 | Creep | 100 | 350 | 10 | – | 0.1 | Broken | |
| G2 | | | 100 | 150 | 10 | 0.12 | 40,961 | Interrupted | |
| G3 | | | 100 | 180 | 10 | 0.17 | 12,628 | Interrupted | 0.8 |
| G4 | | | 100 | 210 | 10 | 0.34 | 75 | Interrupted | |
| G5 | | | 100 | 240 | 10 | 1.07 | 75 | Interrupted | 2.1 |
| G6 | | | 100 | 210 | 600 | 0.31 | 11,907 | Interrupted | |
| G7 | | | 100 | 240 | 600 | 0.65 | 11,787 | Interrupted | |
| T3B | I55 | Creep | 125 | 240 | 3 | 0.37 | 7,245 | Interrupted | 0.8 |
| T4B | | | 125 | 260 | 3 | 0.76 | 7,210 | Interrupted | 0.8 |

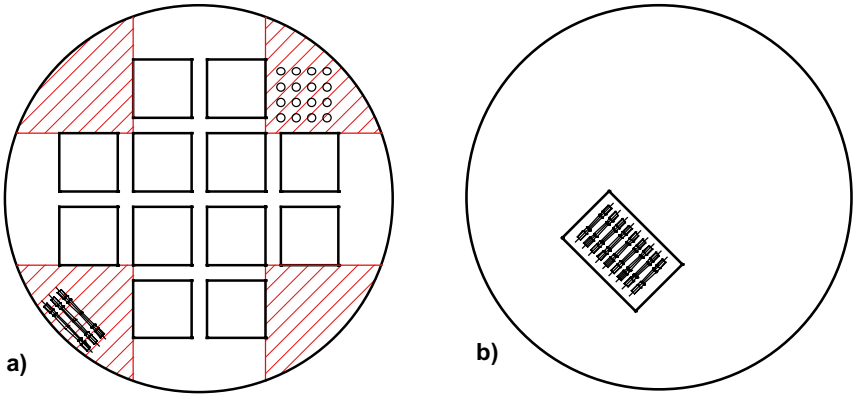


***Figure 3-1.*** *Extraction of creep specimens from the inserts. a) Axial (GAE1-6) and tangential (T3B, T4B) specimen blanks from insert I55; b) Radial (G1-6) specimen blanks from insert I30.*

## 3.2 Metallography and hardness

The creep specimens tested at 100°C were sectioned, ground, polished and the surface etched in 2% Nital to bring out the grain boundaries and different phases in the material. Nital is a solution of nitric acid and ethanol commonly used to etch low alloyed steels to reveal the microstructure. Axial sections along the gauge length, cross-section of the gauge length and cross-section of the thread were examined for each specimen in scanning electron microscope (SEM) and light optical microscope (LOM). The chemical analyses were made with a Link ISIS system at 15 kV. The graphite nodules were quantitatively analysed with respect to size, shape and spacing. Hardness testing was performed after the metallographical studies. The cut-ups with the axial section along the gauge length and the cross-section of the thread were included in this part of the study. Vickers hardness was measured at 100 g. The purpose was to measure the microhardness in the ferritic matrix.

# 4 Results

## 4.1 Creep tests at room temperature; acoustic emission measurement

The initial part of the creep curves of the specimens tested at room temperature are shown in Figure 4-1.

There is an apparent primary creep phase for about 10 h. After that the creep strain is small. This type of primary creep is not observed at the other testing temperatures. The reason for the presence of the primary creep is not known.

In Figure 4-2 the corresponding creep curves with the primary creep removed are shown. The creep strain approximately increases linearly with logarithm of time. This is called logarithmic creep. The creep strain in Figure 4-2 is quite small. The magnitude of the creep strain is not much larger than the uncertainty in the creep strain measurement. This is the reason for the scatter in Figure 4-2. The increase in strain with time after 10 h is quite small compared with the strain during the primary creep, Figure 4-1. At longer time the strain is so small that it might be thought that the creep has stopped altogether, but this is obviously not the case, Figure 4-2. This is a characteristic feature of logarithmic creep. The specimens were all stopped when they reached just under 2,300 hours due to the slow increase in the creep strain.

The total strain in Figure 4-1 increases with the stress. This is, however, not the case for the logarithmic creep strain in Figure 4-2. This observation will be further analysed in the discussion.

A discord sound was heard during loading of the 100°C specimens, see Section 4.2. The origin of the sound could not be determined at the time. For this reason a sensitive microphone was placed against the creep specimens at room temperature during loading. No sound could be registered either by the microphone or the people standing in the room. The explanation for why no sound was heard could be that cast iron from another insert (I55 vs. I30) was used, or that the previous sound emanated from the test setup and that this had been changed inadvertently for this testing. One test was loaded at 100°C to check if the elevated temperature caused the sound, but loading of this specimen was silent too. This extra test specimen was not allowed to continue in creep.

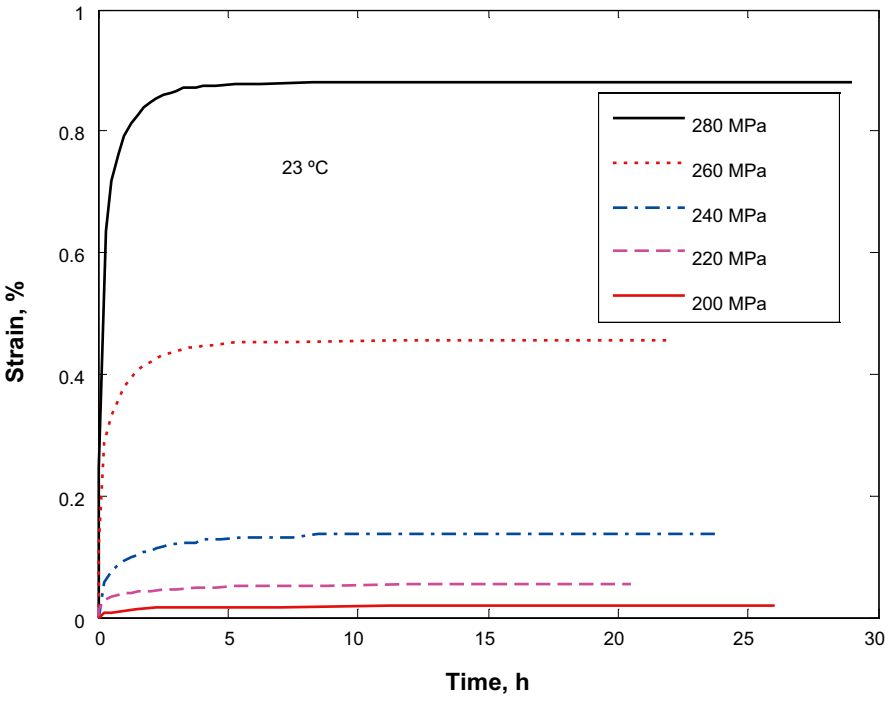


***Figure 4-1.*** *The initial part of the creep curves for tests at room temperature. Insert I55.*

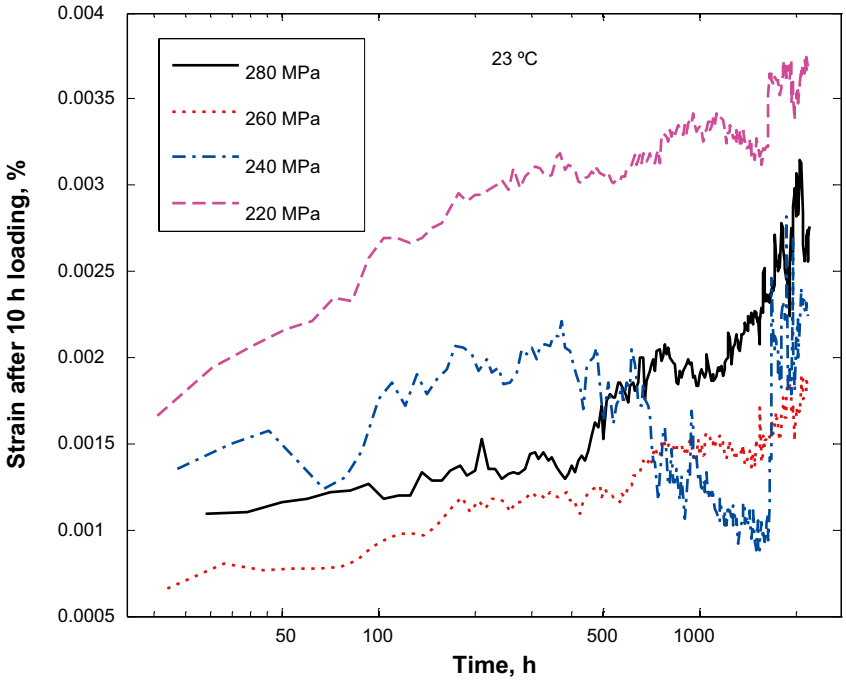


***Figure 4-2.*** *The creep strain is plotted versus time in logarithmic scale with the strain before 10 h loading removed. Room temperature. Insert I55.*

## 4.2 Creep tests, 100°C

In order to reproduce the expected conditions during long term storage, creep tests were carried out at 100°C. The load was applied gradually until full load was achieved after 10 minutes. During the loading of G1 (350 MPa), see Table 3-1, a discord sound audible to the naked ear appeared with its maximum around a stress of 100 MPa. Since the specimen is fixed to the holder by a screw-thread, an explanation implying a sliding of the specimen could be ruled out. The underlying cause was therefore believed to be caused by internal crack formation. A new set of specimens were started, G2 to G5. Specimen G4 (210 MPa) and G5 (240 MPa) were interrupted shortly after full loading. This was done partly due to the lack of creep but it was as well desirable to investigate the effects of the loading on crack formation. A new pair of specimens – G6 (210 MPa) and G7 (240 MPa) – was therefore started with the same parameters as G4 and G5 except for loading time that was changed from 10 min to 10 h. It was found that the discord sound was fainter in the latter tests.

The load applied to G1 (350 MPa) was 20 MPa below the nominal tensile strength at room temperature. Nevertheless it broke during loading at around 200 MPa, even before the load corresponding to the yield strength was attained. The results from the creep tests are shown in Figure 4-3. Four of the specimens have run for more than a year, but they were then interrupted because their creep rates approached zero. In Figure 4-3 the curves are presented without the initial loading strain as in all the diagrams, see Table 3-1, hence only showing the creep strain.

In Figure 4-3 it can be seen that the creep strain increases approximately linearly with the logarithm of time in the same way as in the tests at room temperature. The loading strains are much larger than the creep strains, see Table 3-1. The loading strains increase with stress. However, the creep strains do not after longer testing times. This is the same situation as at room temperature. The highest load gives the highest creep strain while the second highest creep strain is attributed to the specimen with the lowest load.

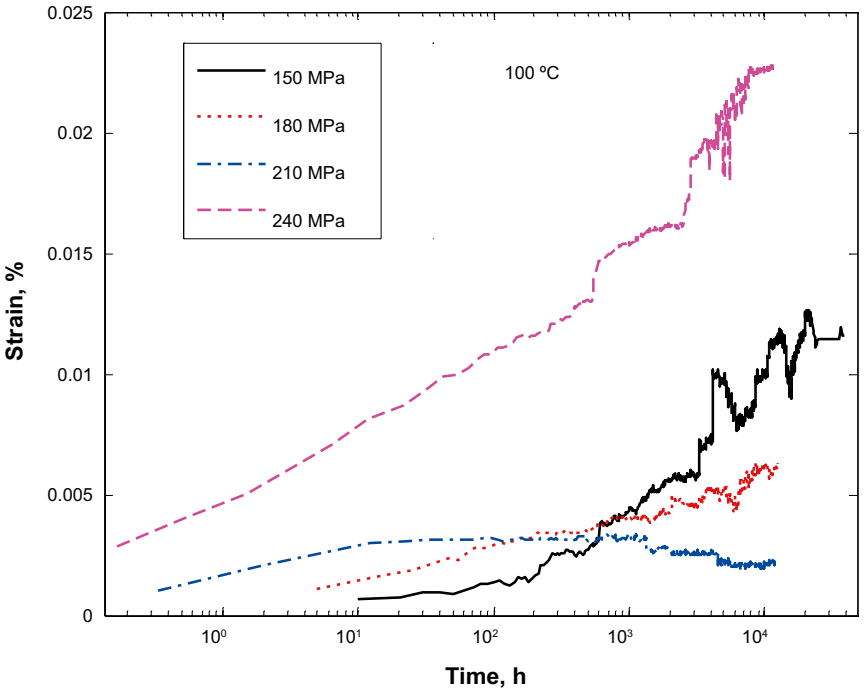


***Figure 4-3.*** *Creep curves for the 100°C specimens. The creep strain is plotted versus time in logarithmic scale. Insert I30.*

## 4.3 Creep tests, 125°C

The temperature of the cast iron insert is estimated to reach a maximum of approximately 125°C during the initial years of the containment. Two specimens were run to verify that the creep properties at 125°C did not differ significantly from those at 100°C. The results are given in Figure 4-4.

It is evident from the results that the 125°C specimens do not creep at a higher rate than at 100°C at longer times. Both tests at 125°C are consistent with logarithmic creep.

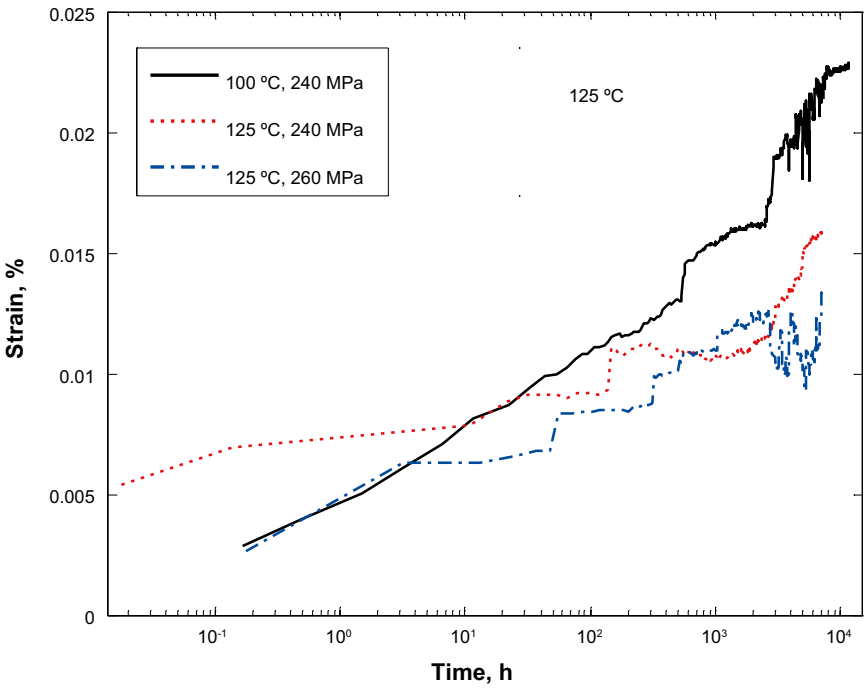


***Figure 4-4.*** *Creep curves for the 125°C specimens. Insert I55. Specimen G7 (100°C/240 MPa) has been included for comparison (insert I30).*

## 4.4 Hardness test

The hardness tests were performed on the same surfaces on the tested specimens that were examined in different microscopes. The results are presented in Table 4-1. Figure 4-5 illustrates where the hardness measurements were performed. Indentations were made at the gauge length, both in the middle of it and closer to the threads. Indentations were also made at the cross-section of the threads.

Some of the measurements differed significantly within the same testing area. For example, the indentations made with the load of 100 g at the centre of the gauge length for specimen G3 had a hardness that varied from 116 to 206 HV0.1. The hardness results from the thread of specimen G7 varied from 122 to 201 HV0.1. This large variation is probably due to the presence of the graphite nodules. As explained above, the indentations were only made in the ferritic matrix. However, an underlying graphite nodule could easily alter the hardness for a specific indentation.

## 4.5 Metallographic examination

### 4.5.1 Graphite examination

The nodules were analysed both at the cross-section of the thread and the axial section of the gauge length. Several light optical microscope (LOM) images were randomly taken at both areas on the unetched, polished surface. Figure 4-6 shows one example.

The total number of measured graphite particles in each area is between 1,265 and 2,313. The number of examined particles gives a relative error of < 0.028 which is acceptable. The relative error is estimated by use of Equation 4-1

$$Relative\ error = \frac{1}{\sqrt{n}} \qquad 4\text{-}1$$

where n is the number of particles measured in the study. The results are presented in Table 4-2. The measurements include the diameter of the nodules, the aspect ratio i.e. the shape of the nodules as the ratio length through width, the spacing i.e. the distance to the nearest neighbour and the area fraction that the graphite occupies.

**Table 4-1. Results from hardness tests.**

| | Creep stress, MPa | Gauge length, closer to the threads, HV0.1 | Std dev | Centre of the gauge length, HV0.1 | Std dev | Thread, HV0.1 | Std dev |
|---|---|---|---|---|---|---|---|
| **G3** | 180 | 190 | 13 | 179 | 27 | 174 | 9 |
| **G6** | 210 | 188 | 9 | 190 | 14 | 187 | 15 |
| **G7** | 240 | 191 | 10 | 189 | 10 | 176 | 20 |

Average from 5 or 10 indentations. Hardness tests in the ferritic matrix.

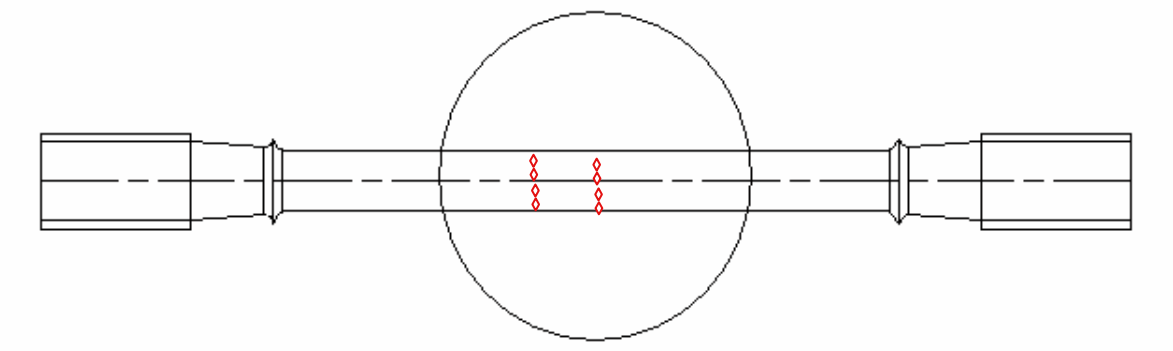

***Figure 4-5.*** *The circular marking shows the part of the specimen that was sectioned, mounted and polished. The rhombus illustrate where the indentations were made.*

**Table 4-2. Results from graphite analysis of creep tests at 100°C.**

| | | G3 gauge length | G6 gauge length | G7 gauge length | G3 thread | G6 thread | G7 thread |
|---|---|---|---|---|---|---|---|
| **Max diameter, µm** | **Max** | 479 | 535 | 655 | 552 | 598 | 476 |
| | **Min** | 15.5 | 15.5 | 16 | 15.5 | 16 | 14.9 |
| | **Average** | 86.9 | 94.9 | 88 | 100 | 102 | 73.7 |
| **Aspect ratio** | **Max** | 4.5 | 5.6 | 5.7 | 4.5 | 5.3 | 4.8 |
| | **Min** | 1 | 1 | 1 | 1 | 1 | 1 |
| | **Average** | 1.4 | 1.5 | 1.4 | 1.4 | 1.4 | 1.4 |
| **Spacing, µm** | **Max** | 2,135 | 2,112 | 2,237 | 2,573 | 2,529 | 2,208 |
| | **Min** | 25.1 | 26 | 26 | 26 | 26 | 25.1 |
| | **Average** | 315 | 328 | 333 | 314 | 341 | 273 |
| **Area fraction** | **Max** | 15.4 | 15 | 14 | 18.4 | 16.5 | 15.1 |
| | **Min** | 12.1 | 11.9 | 11.2 | 12.2 | 9.5 | 11.8 |
| | **Average** | 13.7 | 13.8 | 12.6 | 15.7 | 12.9 | 13.5 |

Specimen from insert I30.

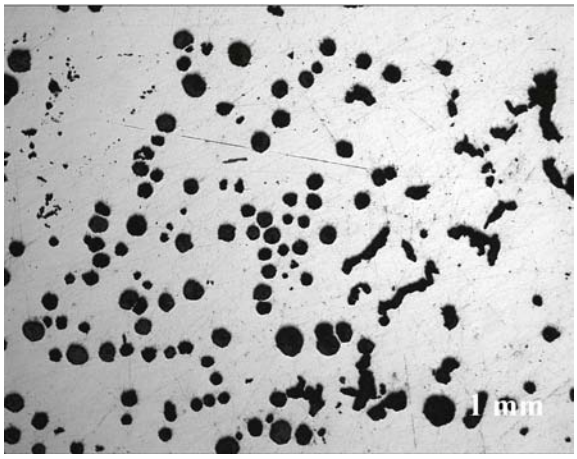


***Figure 4-6.*** *Image taken from the gauge length of specimen G6, creep tested at 100°C. LOM. Insert I30.*

A qualitative examination of the images reveals a heterogeneous distribution of the graphite. There are large areas with only small nodules. Large nodules are found either among equals but at larger spacing than the small nodules or mixed with compacted graphite. Furthermore there are areas with no graphite at all. There is no evident connection between a specific area and where in the specimen it was located. Nor is there any visible difference between the specimens.

### 4.5.2 Microstructure

The microstructure of the creep tested material was documented in both light optical microscope (LOM) and scanning electron microscope (SEM). The results are given in Figure 4-7 to Figure 4-13.

The grain size of ferrite was estimated from the LOM images. The average grain size at the gauge length of the specimen was near 100 µm for G3 and G7 and 140 µm for G6. There is a large variation in grain size for all three specimens. The grain size in G3 ranges from 70 to 160 µm, in G6 from 60 to 290 µm and in G7 from 20 to 200 µm. As expected the grain size in the unstrained material, i.e. the thread, is the same.

The morphology is similar in all examined specimens. The microstructure contains spheroidal graphite mixed with compacted graphite while the grain size varies with the distribution of the graphite. Compacted graphite is quite frequently occurring, although the greater part of the present graphite belongs to type V or VI. The internal distance between the smaller graphite nodules is shorter than the distance between the larger nodules.

Another similarity is the existence of pearlite in the ferritic matrix (see Figure 4-7 and Figure 4-8). In the latter image, a pore is visible in the pearlitic phase, which was the only one detected in the examined specimens in the regions not affected by creep load. No microcracks or voids adjacent to graphite or pearlite have been found, or in any other location of the examined material.

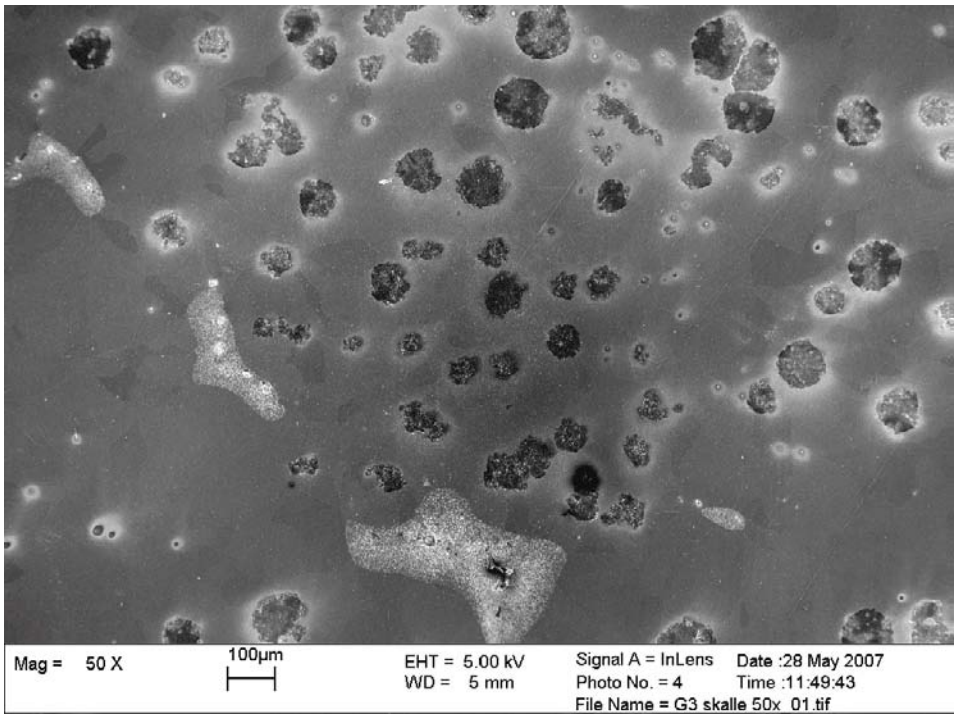


***Figure 4-7.*** *SEM micrograph from the thread of specimen G3 (insert I30). The image is from an area with a pearlitic content above average. The form of the graphite ranges from type III (compacted graphite) to type VI (spheroidal graphite).*

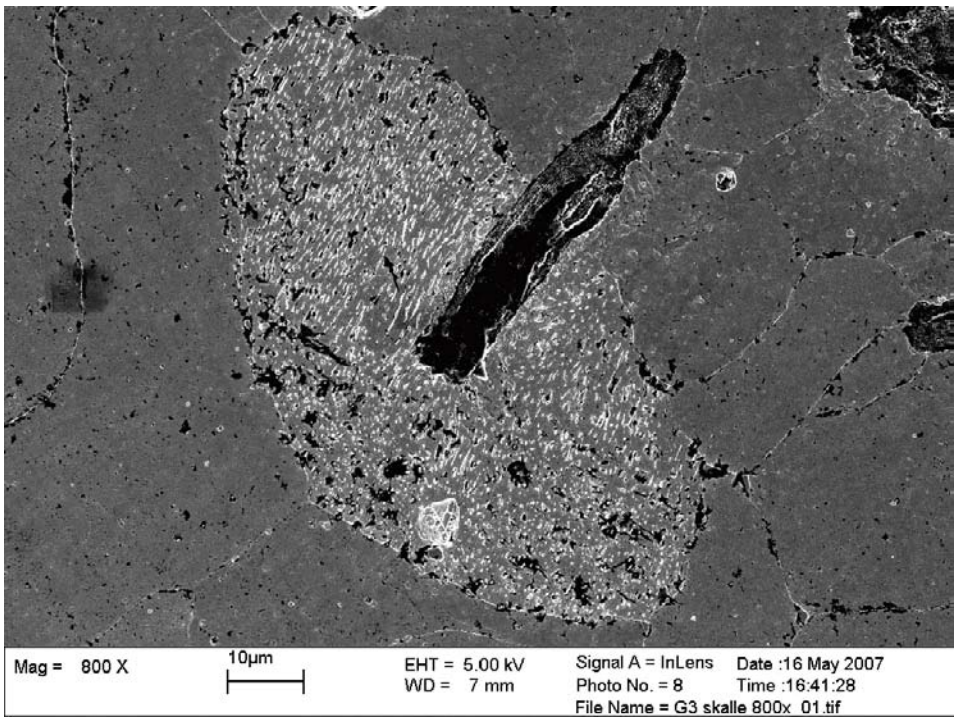


***Figure 4-8.*** *SEM micrograph from the thread of specimen G3 (insert I30) showing a pearlitic grain in the ferrite with a pore. This was the only pore found during the examination of material not exposed to creep load.*

Figure 4-9 shows a typical distribution of graphite of different forms: the area with compacted graphite separated from the nodular graphite. Specimen G6 (210 MPa) did not only have areas with pearlitic structure (see Figure 4-10). A closer look in Figure 4-11 reveals that the composition in between these areas differs from the matrix. The results from the chemical analysis are presented in the Section 4.5.3.

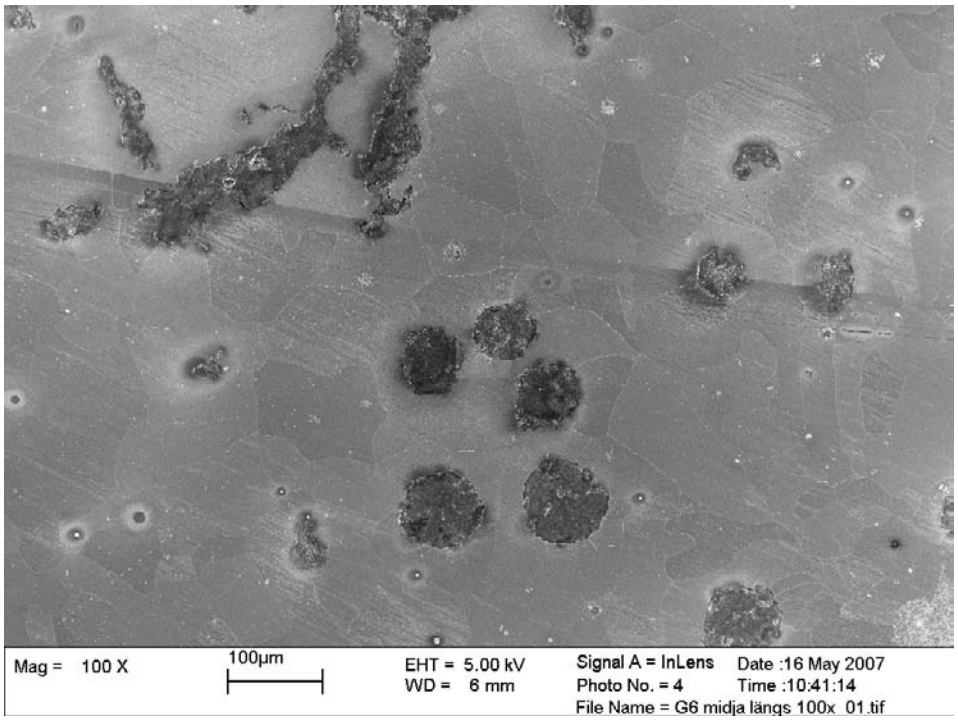


***Figure 4-9.*** *SEM micrograph from the gauge length of specimen G6 (insert I30) showing both compacted and spheroidal graphite only a few grain sizes apart.*

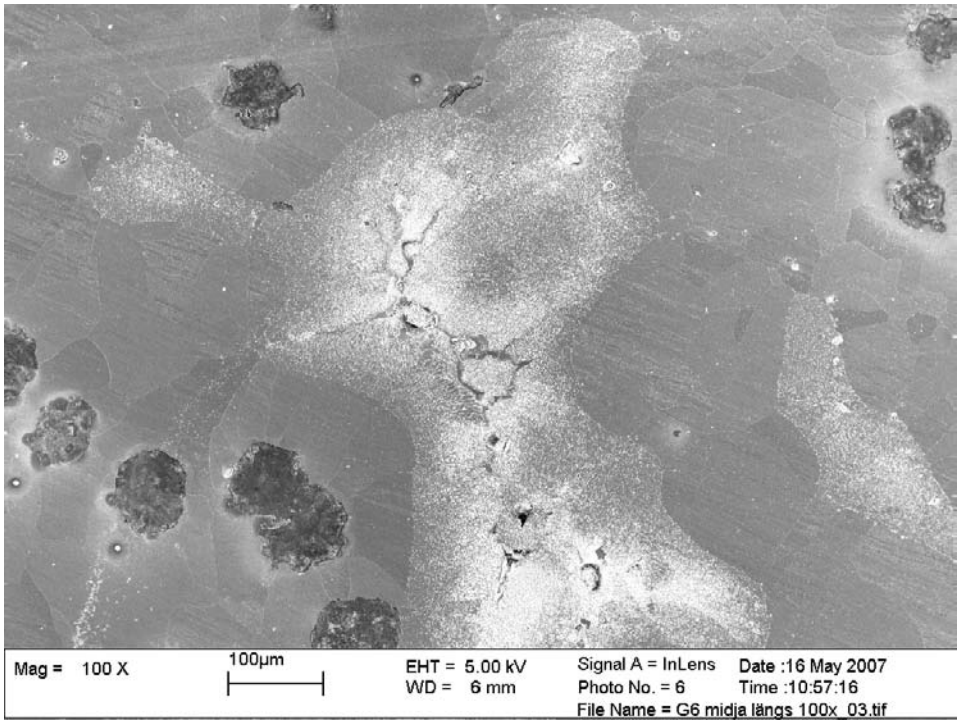


***Figure 4-10.*** *SEM micrograph from the gauge length of specimen G6 (insert I30). A large, continuous area of pearlite around a cell boundary.*

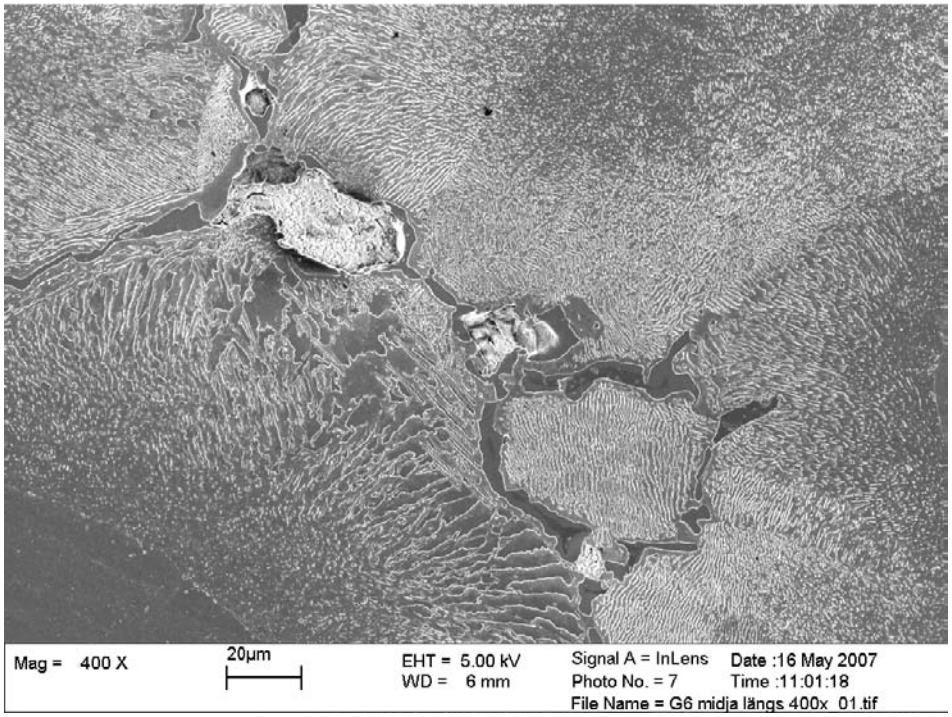


***Figure 4-11.*** *SEM micrograph from the gauge length of specimen G6 (insert I30). A close-up of Figure 4-10 shows the cell boundary.*

Figure 4-12 and Figure 4-13 well describe the microstructure in G7 (240 MPa). The first one displays a typical microstructure with large nodules mixed with compacted graphite or graphite of irregular shape while the latter presents a distinguished demarcation between the compacted graphite and the small nodules.

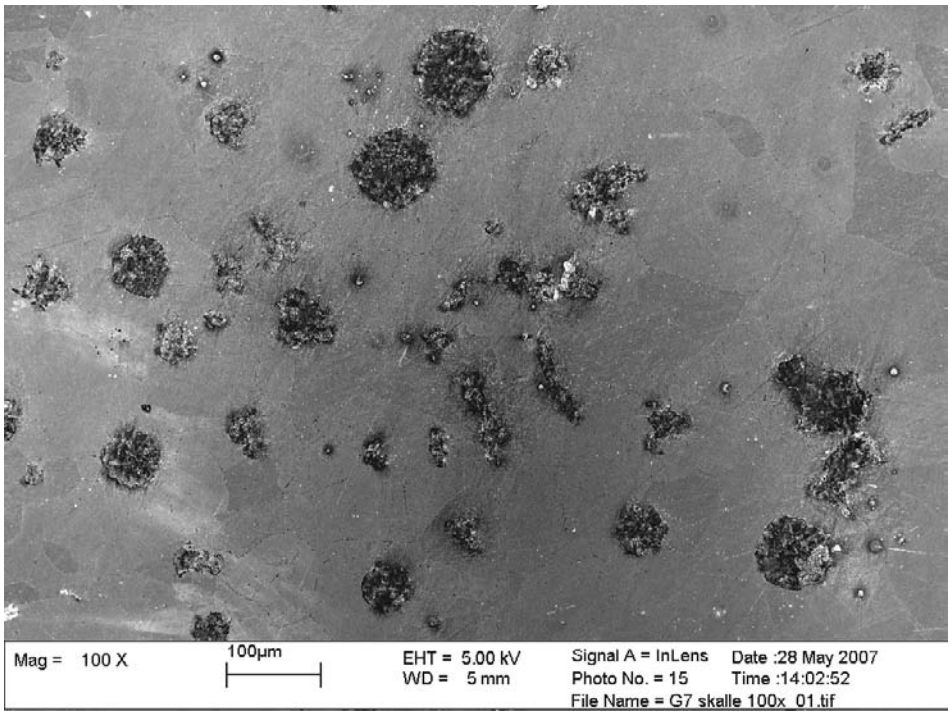


***Figure 4-12.*** *SEM micrograph from the thread of specimen G7 (insert I30). The variation in graphite form from type III to type VI is found in all examined specimens. Here, large spheroidal graphites are mixed with compacted graphite.*

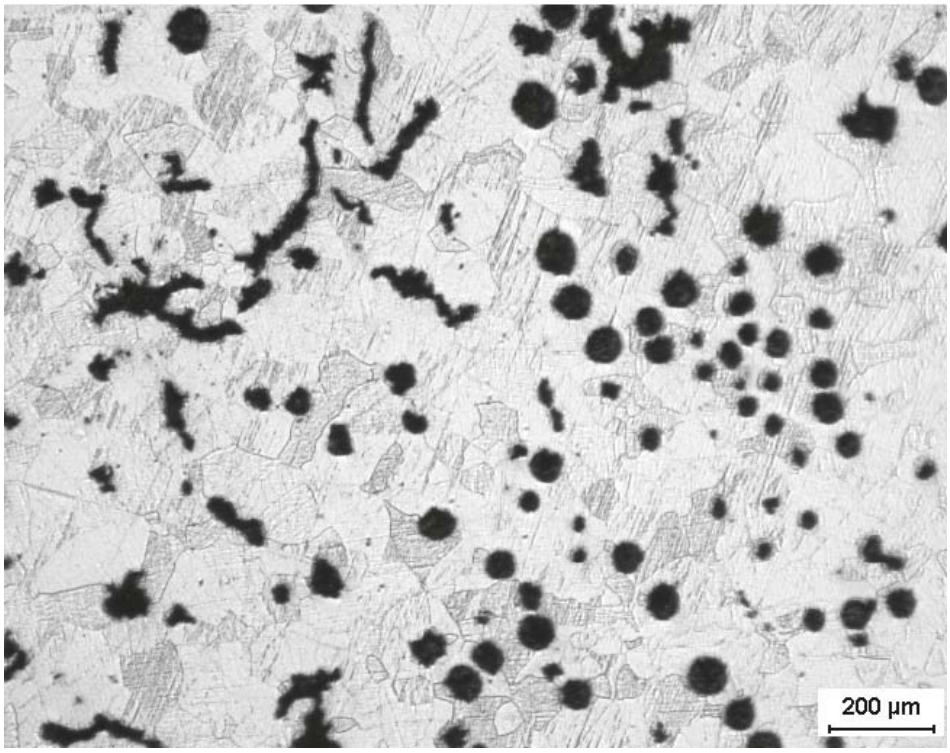


***Figure 4-13.*** *LOM micrograph from the thread of specimen G7 (insert I30) showing a typical microstructure with a large area of spheroidal graphites separated from the compacted graphite.*

### 4.5.3 Chemical composition of particles

Areas with pearlitic phase were present in all the examined specimens. A distinguishing feature for the larger areas was a darker phase of long, narrow shape localised within the pearlite. Figure 4-14 and Figure 4-15 show the exact positions where the analyses were made. The results are found in Table 4-3. The limitations of the analysis system has to be taken into consideration, i.e. that the experimental set-up is not able to quantitatively determine the presence of C or elements with lower atomic mass. It is interesting to notice that while the composition at point 2 and 3 is very similar to the matrix, the main element at point 1 is vanadium and at point 4 vanadium together with titanium.

**Table 4-3. Result from the chemical analysis.**

| No | Cr | Fe | Mn | S | Si | Ti | V |
|---|---|---|---|---|---|---|---|
| **1** | | 2.40 | | 1.51 | | 3.60 | 92.49 |
| **2** | 1.03 | 92.29 | 1.79 | (0.28) | | | 4.61 |
| **3** | (0.48) | 96.40 | (0.41) | (0.04) | 2.40 | (0.10) | (0.17) |
| **4** | (0.65) | 3.99 | (0.10) | 1.75 | (0.46) | 23.13 | 69.92 |

The values in brackets are below the accuracy of the analysis system.
Carbon, nitrogen, and oxygen are not analysed.

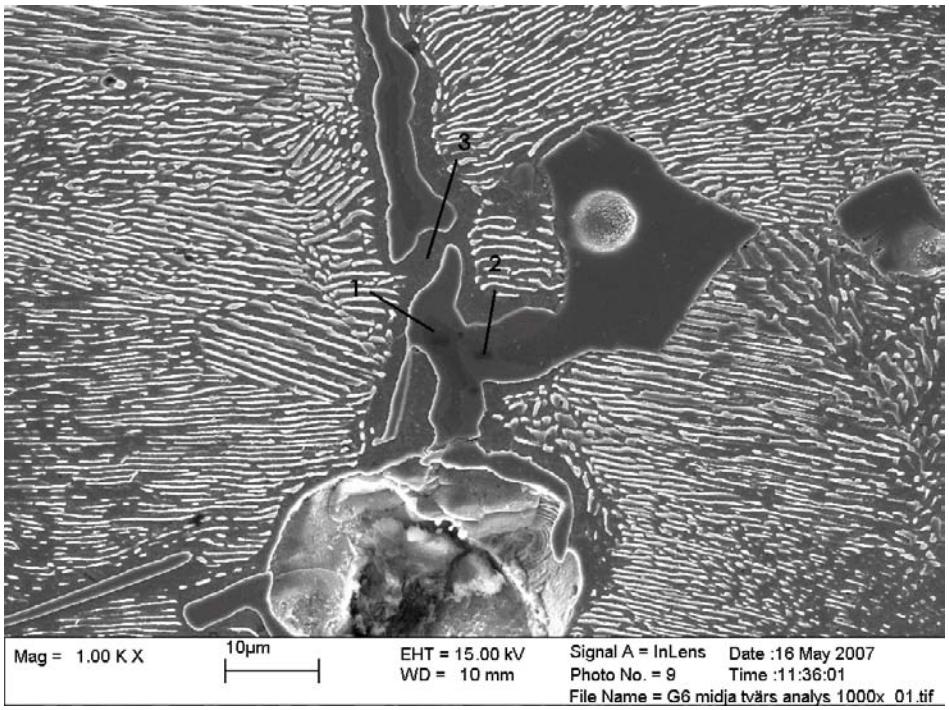


***Figure 4-14.*** *SEM micrograph from the gauge length of specimen G6 (insert I30). The analysed areas are denoted from No 1 to 3.*

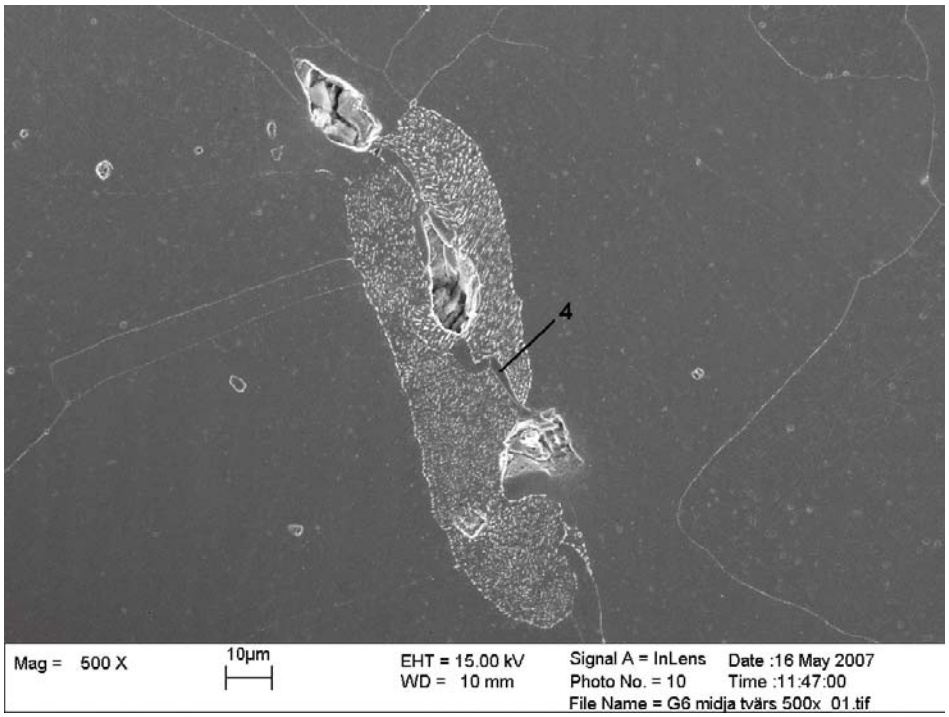


***Figure 4-15.*** *SEM micrograph from the gauge length of specimen G6 (insert I30) showing pearlite. The analysed area is denoted with No 4.*

# 5 Discussion

The results from the creep testing of nodular cast iron have shown that for none of the tested stresses, the creep strain is more than 0.025% at 100 or 125°C. The shape of the curves implies that the creep behaviour is generally logarithmic in nature. The same applies to the tests at room temperature for times exceeding 10 h, if the strain appearing before this time limit is subtracted. In this case the maximum creep strain is even less, < 0.004%.

The definition of logarithmic creep is that the creep strain is linear in the logarithm of the testing time. This can be seen as a straight creep curve when viewed in logarithmic time scale. It implies that the creep rate decreases very rapidly with increasing time, eventually reaching such a low value that it cannot be measured any longer.

Many researchers believe that logarithmic creep is primary creep that does not reach the secondary or tertiary stage within accessible testing times. In fact, this is fully consistent with the W model for primary creep /12/.

$$\dot{\varepsilon} = Ae^{-k\varepsilon} \qquad 5\text{-}1$$

where $\dot{\varepsilon}$ is the creep rate, e the creep strain and $A$ and $k$ constants. If Equation 5-1 is integrated it gives the following time dependence

$$\varepsilon = \frac{1}{k}\ln(Akt + e^{k\varepsilon_0}) \qquad 5\text{-}2$$

where $e_0$ is the initial creep strain. This is precisely the type of logarithmic time dependence that has been observed for cast iron in the present report. The W model is known to describe primary creep for example for 9% Cr steel /13/ and 12% Cr steel /11/.

The implications of the logarithmic creep behaviour are far reaching. Experimentally the creep strain does not exceed 0.01% per factor of 10 in time. If the logarithmic creep prevails at very long times, the creep strain will not exceed 0.1% even for design times of interest for the KBS-3 nuclear waste package. To this loading strains of up to about 1% should be added.

Literature data on logarithmic creep is scarce and exists mainly for shorter testing times. Here a comparison is made to the data by Usami et al. /8/. In order to determine the effect of the stress level on the logarithmic creep strain, $e_c$ was introduced as the creep strain at $10^5$ s. This creep strain is plotted versus a normalised stress, which is the creep stress divided by the yield strength, Figure 5-1.

In Figure 5-2 the creep data for nodular iron from the present investigation are shown in the same way. The amount of creep strain at $10^5$ s (27 h) is in the interval $3\times10^{-5}$ to $9\times10^{-4}$ at room temperature, $10^{-5}$ to $10^{-4}$ at 100°C and $6\times10^{5}$ to $9\times10^{-5}$ at 125°C.

Figure 5-1 and Figure 5-2 have similar scales on the axes in order to facilitate the comparison. According to Table 2-2 the yield strength at room temperature is 276 MPa. At 125°C a value of 244 MPa has been measured /SKBdoc 1207576/. The yield strength at 100°C is interpolated to 251 MPa from the values at room temperature and 125°C. The alloy closest to nodular iron in creep behaviour in Figure 5-2 is the low-alloyed steel, encircled in red.

From Figure 5-2 it is evident that the creep strain at 27 h is of the same order of magnitude as for the low alloy steel. The creep strain at this time increases with increasing stress level. It seems that stress dependence is somewhat weaker for the nodular iron in comparison to the low alloy steel. At 23°C, cases with and without primary creep before 10 h are shown. The data for the low alloy steel is closer to the total strain at 23°C at high stresses but more comparable to the strain after 10 h at lower stresses. This can possibly be related to a difference in the ratio between the primary strain and the loading strain. For the low alloy steel this ratio is smaller than for the nodular iron at low stresses but more comparable at higher stresses.

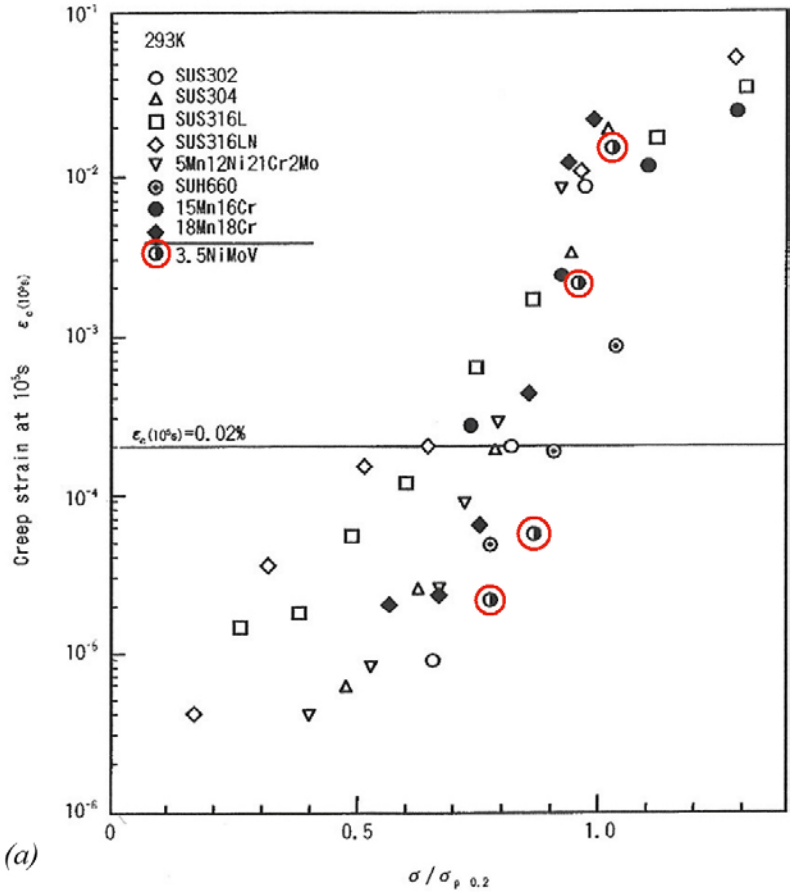


***Figure 5-1.*** *Creep strain at $10^5$ s, $\varepsilon_c$ ($10^5$ s), versus normalised stress for austenitic steels and low-alloyed steel (encircled in red) at 20°C /8/.*

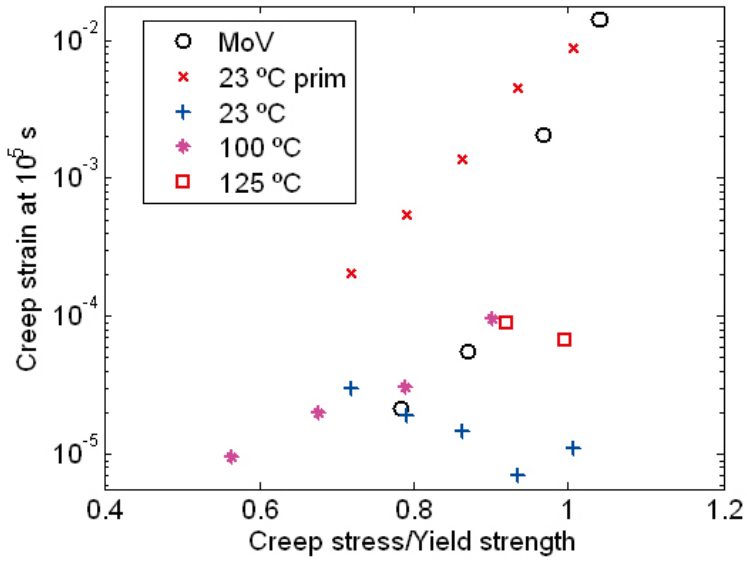


***Figure 5-2.*** *Creep strain at $10^5$ s (27 h) versus the ratio between creep stress and yield strength for nodular iron at 23, 100 and 125°C. At 23°C the effect of including primary creep is also shown. A comparison is made to a low alloy MoV steel at room temperature /8/. Yield strength values for insert I55 used.*

The slope of the creep curves in Figure 4-2 to Figure 4-4 is described by the constant k in Equation 5-1. When the slope is reasonably constant in these Figures, the value k has been determined. The values are included in Table 3-1. At room temperature k is $2–4\times10^{-6}$. At 100°C it is $0.8–2\times10^{-5}$ and at 125°C it is $6–8\times10^{-6}$. The k value is thus slightly higher at 100 and 125°C than at room temperature. There is no clear stress dependence of the k value. At 23°C, the low stress 220 MPa gives the highest k, whereas at 100°C the high stress 240 is also associated with a high k.

The steady diminution of creep strain for specimen G6 (100°C, 210 MPa) after a little more than 1,000 hours is small but notable, see Figure 4-3. The maximum value of the creep strain of G6 is 0.0031% and the value at the interruption is only 0.0019%. This is of the same order as the experimental uncertainty in the results, which can be explained in the following way. During the test, temperature was controlled within ± 2°C of test temperature. Actually, the permitted temperature fluctuation is +3°C /14/. The change in strain with temperature is determined by Equation 5-3.

$$\delta = \alpha \cdot \Delta T \qquad 5\text{-}3$$

$\alpha$ is the coefficient of thermal expansion = $11.2\times10^{-6}$ $K^{-1}$ in the temperature interval 20–110°C, $\delta$ the change in strain of the specimen, and $\Delta T$ temperature change = 2°C. A decrease in temperature with only 2°C would give $\delta$ = 0.002%. This change is twice as large as the actual observed decrease in creep strain.

The effect of temperature fluctuation on creep strain variation can be seen in Figure 5-3 and Figure 5-4 for the 125°C specimens. For the tests at 240 MPa, see Figure 5-3, the temperature is fairly constant during the test, which results in a weak, steady increase of creep strain. For the tests at 260 MPa, see Figure 5-4, the creep strain decreases/increases with decreasing/increasing temperature, although the temperature is controlled within the permissible range.

The acoustic emission tests at room temperature showed that no discord sound could be heard during the loading of the specimens. This suggests that the sounds heard during the loading of the 100°C specimens emanated from the load train or the test rig or were intrinsic to that particular insert. If so, they could be related to the nodule distribution and morphology.

The largest load on the canister and hence on the insert is expected to happen during glaciations when the temperature of the cast iron is estimated to be about 0°C. It is known that the strength in general increases with decreasing temperature below room temperature. Consequently the creep rates can be expected to be equivalent or lower at 0°C in comparison to the room temperature values.

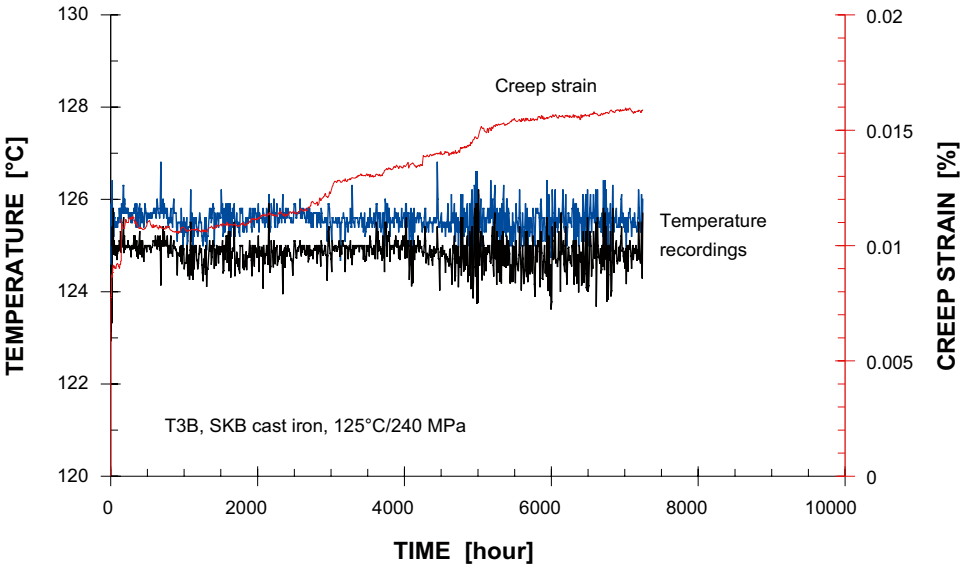


***Figure 5-3.*** *Temperature and creep strain as a function of time for the specimen T3B at 125°C/240 MPa.*

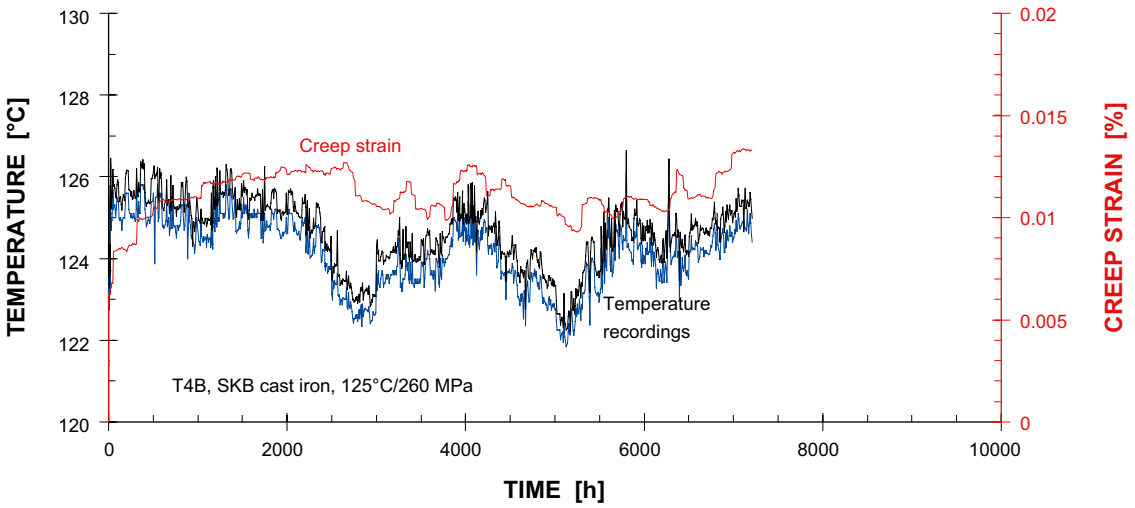


***Figure 5-4.*** *Temperature and creep strain as a function of time for the specimen T4B at 125°C/260 MPa.*

In general, the creep strain increases with the applied load at a given temperature. This is, however, only observed after shorter testing times but not after longer ones. There is no change in the ferrite grain size or the graphite nodules during creep deformation. The ferrite grain size of the three examined creep specimens at 100°C is approximately the same, although the range is extended. There is no systematic difference in nodule size or shape that could affect the creep deformation. Pearlite was observed in all specimens. No microcracks were detected, which had been assumed originally to cause the discord sound during loading. It has been reported /8/ that vanadium, titanium and silicon are some of the most effective solute elements in ferrite. They improve the creep resistance at higher temperatures by reducing the dislocation energy.

The specimens show a homogeneous hardness over the entire cross-section. The hardness in the unstrained material, i.e. the thread, was slightly inferior or similar. The hardness results showed no tendency to depend on the creep stress. In conclusions it is unlikely that variations in the microstructure could explain the stress dependence of the creep strain.

Another possible explanation about the influence of the stress on the creep strain is related to the loading strain. It is observed that a high loading strain is coupled to a lower creep strain at long times. There is one major exception and that is the G7 specimen (100°C, 240 MPa). It seems that the “remaining” loading strain can be transferred into creep strain at longer times.

One of the demands on the material is that a high fraction of the graphite ($\geq$ 80%) should be of nodular shape (form V and VI in /11/). The graphite examination shows that the amount of graphite particles with an aspect ratio exceeding 2.0 is less than 11%. Only the microstructure of insert I30 was studied in this investigation. For an aspect ratio $\geq$ 1.5 the quotient is 26%. According to previous tests in cast iron /8/ the effect of the temperature on the graphite growth is negligible below 400°C. Consequently the nodule size is a result of the casting. Liu et al. /15/ emphasize the importance of an optimal nodule size. They showed that large nodular graphite results in rapid void growth. Thus, the strength and the ductility are deteriorated.

# 6 Conclusions

Nodular cast iron intended for the canister insert for spent nuclear fuel disposal has been creep tested at room temperature, 100 and 125°C for up to 41,000 h.

- The creep behaviour of the nodular iron is logarithmic in nature at all test temperatures. The creep strain after the loading phase is always very small. The maximum creep strain recorded was 0.025%.
- Logarithmic creep technically implies that the creep strain rate is so low at longer times that it cannot be measured anymore. It can be estimated that the total creep strain would be less than 0.1% even after very long times of the timescale of the repository.
- Logarithmic creep can be considered as a special type of primary creep that never reaches the secondary stage. The W-model for primary creep gives in fact precisely the time dependence that is observed during logarithmic creep.
- Since stress levels up to 15% above the nominal minimum yield strength have been covered in the creep tests, the small recorded creep strains imply that they are technically insignificant.
- The discord sounds that could be heard during initial experiments were not audible in further experiments.
- No recurrent porosity or voids could be found in the material.
- The hardness in the unstrained material, i.e. the threads, was slightly inferior or similar to the hardness in the gauge length.
- Graphite examination of the tested material from insert I30 shows that the amount of graphite particles with an aspect ratio exceeding 2.0 is less than 11%. For an aspect ratio $\geq$ 1.5 the quotient is 26%.
- All examined specimens contained a small amount of pearlitic phase, preferentially located at the grain boundaries.

# 7 Acknowledgements

The authors wish to thank Svensk Kärnbränslehantering AB (SKB) for funding this work and supplying the test material. Swerea Swecast is thanked for carrying out the tensile tests, the Brinell hardness measurements, and graphite characterisation of the original cast iron material.

# 8 References

SKB's (Svensk Kärnbränslehantering AB) publications can be found at www.skb.se/publications. References to SKB's unpublished documents are listed separately at the end of the reference list. Unpublished documents will be submitted upon request to document@skb.se.


/1/ **SKB, 2007.** RD&D Programme 2007. Programme for research, development and demonstration of methods for the management and disposal of nuclear waste. SKB TR-07-12, Svensk Kärnbränslehantering AB.

/2/ **SKB, 2009.** Design premises for a KBS-3V repository based on results from the safety assessment SR-Can and some subsequent analyses. SKB TR-09-22, Svensk Kärnbränslehantering AB.

/3/ **SKB, 2006.** Long-term safety for KBS-3 repositories at Forsmark and Lax emar – a first evaluation. Main report of the SR-Can project. SKB TR-06-09, Svensk Kärnbränslehantering AB.

/4/ **Wilks C R, Mathews N A, Kraft R W, 1954.** Elevated temperature properties of ductile cast irons. AFS Transactions 47.

/5/ **Foley F B, 1956.** Mechanical properties at elevated temperatures of ductile cast irons. Transactions of the American Society for Metals, 78, pp 1435–1438.

/6/ **Angus H T, 1969.** Stress resistance of unalloyed and alloyed cast iron at high temperatures and the use of grey, malleable and nodular or spheroidal graphite iron at steam temperatures. The British Foundryman, Nov 1969, pp 407–431.

/7/ **Röhrig K, 1978.** Hitzebeständiges GGG mit 4 bis 6% Si – Eigenschaften und Anwendungen. Konstruieren und Gießen 3, 1978, pp 3–16.

/8/ **Usami S, Mori T, 2000.** Creep deformation of austenitic steels at medium and low temperatures. Cryogenics, 40, pp 117–126 .

/9/ **SS-EN 1563:1997.** Founding – Spheroidal graphite cast iron. Stockholm: Swedish Standards Institute; SS-EN 1563/A1:2002. Founding – Spheroidal graphite cast irons. Stockholm: Swedish Standards Institute.

/10/ **SS-EN ISO 6506-1:2006.** Metallic materials – Brinell hardness test – Part 1: Test method (ISO 6506-1:2005). Stockholm: Swedish Standards Institute.

/11/ **SS-EN ISO 945-1:2008.** Microstructure of cast irons – Part 1: Graphite classification by visual analysis (ISO 945-1:2008). Stockholm: Swedish Standards Institute.

/12/ **Wu R, Sandström R, Storesund J, 1994.** Creep strain behavior in a 12% CrMoV steel. Materials at High Temperatures, 12, pp 277–283.

/13/ **Wu R, Sandström R, Seitisleam F, 2004.** Influence of extra coarse grains on the creep properties of 9 percent, CrMoV (P91) steel weldment. Journal of Engineering Materials and Technology, 126, pp 87–94.

/14/ **SS-EN ISO 204:2009.** Metallic materials – Uniaxial creep testing in tension – Method of test (ISO 204:2009). Stockholm: Swedish Standards Institute.

/15/ **Liu J H, Hao X Y, Li G L, Liu G S, 2002.** Microvoid evaluation of ferrite ductile iron under strain. Materials Letters, 56, pp 748–755.


**Unpublished documents**

| SKBdoc id, version | Titel | Issuer, year |
|---|---|---|
| 1175208 ver 5.0 | Tillverkning av kapselkomponenter. | SKB, 2010 |
| 1207576 ver 1.0 | Test of mechanical properties on cast iron inserts for encapsulation of spent nuclear fuel, summary report. | SKB, 2009 |